Geological Society, London, Special Publications Online First

Stable isotope chemostratigraphy in lacustrine strata of the Xiagou Formation, Gansu Province, NW China

Marina B. Suarez, Gregory A. Ludvigson, Luis A. González, Aisha H. Al-Suwaidi and Hai-Lu You

Geological Society, London, Special Publications, first published May 14, 2013; doi 10.1144/SP382.1

Stable isotope chemostratigraphy in lacustrine strata of the Xiagou Formation, Gansu Province, NW China

MARINA B. SUAREZ[1,6]*, GREGORY A. LUDVIGSON[2], LUIS A. GONZÁLEZ[1], AISHA H. AL-SUWAIDI[3,4] & HAI-LU YOU[5,7]

[1]*Department of Geology, The University of Kansas, 1475 Jayhawk Boulevard., Lawrence, KS 66045, USA*

[2]*Kansas Geological Survey, 1930 Constant Avenue, Lawrence KS 66047, USA*

[3]*Department of Earth Sciences, Oxford University, South Parks Road, Oxford OX1 3AN, UK*

[4]*Present address: Petroleum Institute University and Research Centre, Petroleum Geoscience Dept., PO BOX 2533, Abu Dhabi, UAE*

[5]*Institute of Geology, Chinese Academy of Geological Sciences, 26 Baiwanzhuang Road, Beijing 100037, China*

[6]*Present address: Department of Geological Sciences, University of Texas at San Antonio One UTSA Circle, San Antonio, Texas 78249, USA*

[7]*Present address: Key Laboratory of Vertebrate Evolution and Human Origin of Chinese Academy of Sciences, Institute of Vertebrate Paleontology and Paleoanthropology, Chinese Academy of Sciences, 142 Xizhimenwai Street, Beijing 100044, China*

**Corresponding author (e-mail: Marina.Suarez@utsa.edu)*

Abstract: Two sections from Early Cretaceous lacustrine strata of the Xiagou Formation from the Changma Basin in Gansu Province, China, are correlated based on their carbon isotopic compositions of bulk sedimentary organic matter and carbonate, as well as carbonate oxygen-isotopic compositions. The samples were collected from fossiliferous strata, which contain well-preserved Cretaceous bird remains. The sections are primarily correlated based on a two-step increase in $\delta^{13}C_{org}$ with an overall magnitude of *c.* 12.5‰. The stratigraphic variations in carbon isotopes within the two lacustrine sections are correlated with global carbon isotope variations C3–C7 based on marine carbon isotope records. This correlation places the Xiagou lacustrine strata in this locality within the early Aptian Stage, specifically, the Selli Equivalent, which is associated with Ocean Anoxic Event 1a.

The Lower Cretaceous record of positive and negative $\delta^{13}C$ excursions in organic carbon and carbonate carbon has been well documented (Menegatti *et al.* 1998; Bralower *et al.* 1999) in marine strata. Based on the relationship between carbon reservoirs in the ocean–atmosphere system, variations of $\delta^{13}C$ from organic carbon and carbonate in continental sediments have been used to correlate the continental chemostratigraphic record of these excursions with those in the marine record (Grocke *et al.* 1999; Heimhofer *et al.* 2003; Ludvigson *et al.* 2010). This can be particularly useful in sedimentary sequences, which may have limited means for chronostratigraphic constraints.

Abundant exposures of Lower Cretaceous continental strata occur in Gansu Province, China (Fig. 1), and contain well-preserved flora and fauna, including the remains of dinosaurs, birds and flowering plants (Tang *et al.* 2001; You *et al.* 2005, 2006, 2010; Ji *et al.* 2011). Although palaeontological research in these regions has advanced, detailed stratigraphic relationships and correlations between sites and between local basins are still uncertain. Palaeoenvironmental and palaeoclimatological interpretations are dependent on more accurately defining the stratigraphic succession and timing of these continental deposits.

This study focuses on the Xiagou Formation in the locally named Changma Basin in the northwestern part of Gansu Province (Fig. 1), which has produced a number of well-preserved early bird fossils and is known to be Early Cretaceous in age based on biostratigraphy of purported equivalent strata in the region (see section 'Background

From: Bojar, A.-V., Melinte-Dobrinescu, M. C. & Smit, J. (eds) 2013. *Isotopic Studies in Cretaceous Research*. Geological Society, London, Special Publications, **382**, http://dx.doi.org/10.1144/SP382.1

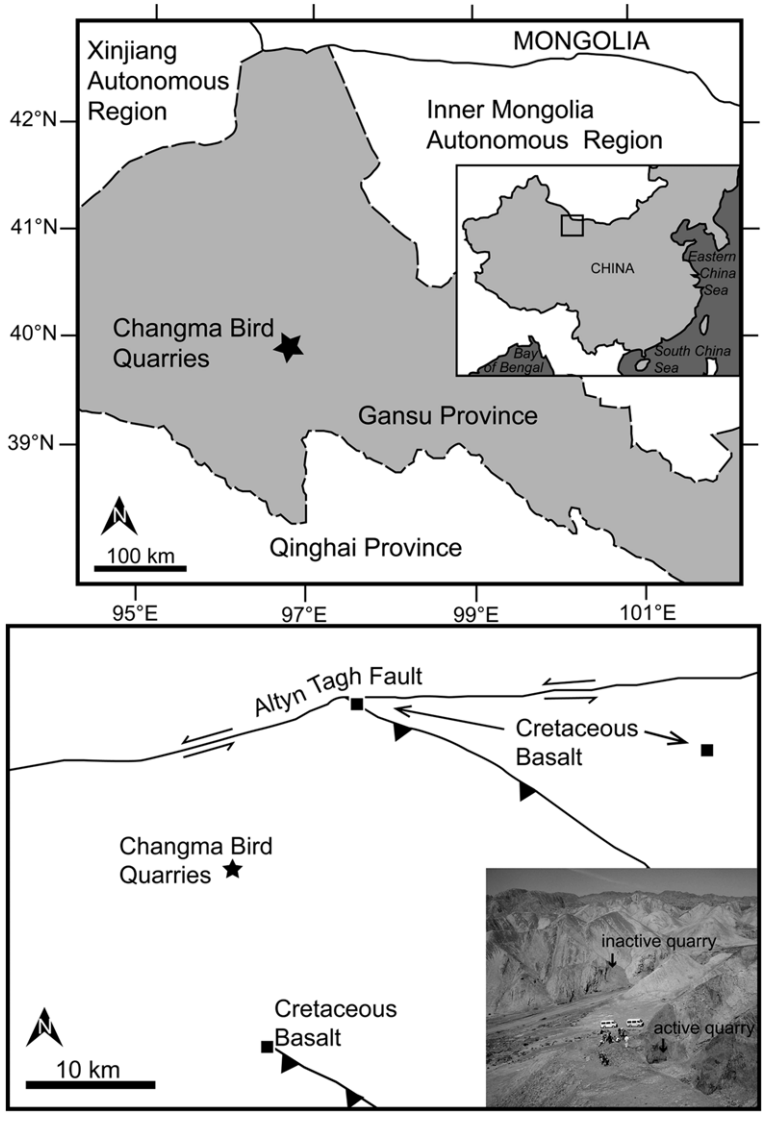

Fig. 1. Location of the Changma bird quarries, and structural geological map. (Modified from Li & Yang 2004.) Inset photograph: location of the two bird fossil quarries.

geology'; You *et al.* 2006). Because detailed temporal relationships in this region are lacking, it is the goal of this study to make use of the stable carbon isotope chemostratigraphy of sedimentary organic carbon to provide better time constraints for an important fossil bird locality.

Background geology

Lower Cretaceous strata in northwestern Gansu Province consist primarily of fluvio-lacustrine strata that were deposited in intermontane basins. These basins formed as numerous tectonic blocks coalesced during the late Palaeozoic to early Mesozoic periods (Frost *et al.* 1995; Chen & Yang 1996; Zhao *et al.* 1996). Samples were taken from the locally named Changma Basin near the town of Changma. The Changma Basin locality is situated in a wedge-shaped basin bounded to the north by the Altyn Tagh strike–slip fault and thrust faults to the east and south (Fig. 1). The basin began to form along the already active Altyn Tagh fault as left-lateral movement caused clockwise rotation of the basin; this,

together with continued uplift to the south, resulted in local subsidence and fault-bounded basins (Li & Yang 2004).

Four formations within this region are thought to span the Early Cretaceous series: the Chijinqiao (sandstones interbedded with mudstones and siltstones), Chijinpu (sandstones interbedded with mudstones and siltstones), Xiagou (mudstones, shales and siltstones interbedded with sandstones) and Zhonggou (sandstones) formations (Chen & Yang 1996; You pers. comm. 2011). Precise ages of these formations are lacking, and biostratigraphic correlations produce only a coarse resolution for ages. As reported in You *et al.* 2006 (and references therein), ostracode and charophyte biostratigraphy from strata thought to be correlative to the lacustrine Xiagou Formation in the Changma Basin suggests a Barremian Age, while pollen suggests a Hauterivian Age. The Xiagou Formation in the Changma Basin has yielded numerous well-preserved fossils of early birds, including *Gansus yumenensis* and *Qiliania graffini* as well as other unnamed early bird specimens (You *et al.* 2005, 2006, 2010; Ji *et al.* 2011). Together with vertebrate material, abundant invertebrates such as conchostracans, ostracodes, charophytes, insects and freshwater mussels are also present, but detailed biostratigraphic analysis from this locality has not been completed. The similarity of taxa found in the Xiagou Formation and the underlying Chijinpu Formation with those found in the Jehol Biota of Liaoning Province suggests a Barremian to Aptian age (He *et al.* 2004; You *et al.* 2006). *G. yumenensis* is thought to be evolutionarily as advanced or more advanced than bird taxa of the Jehol biota (You *et al.* 2006).

No numerical age dates exist for the main fossil localities. Numerical age dates from mafic to intermediate lava flows interbedded with equivalent Cretaceous strata, and dykes cross-cutting Cretaceous strata from localities surrounding the Changma Basin, have been dated using whole-rock K–Ar and Ar/Ar. Figure 1 shows the locality of the lava flows dated and reported by Li & Yang (2004), the majority of which are Aptian (with the exception of the Beidayao locality). The Beidayao locality to the north of the Changma Basin produces a K age of 99.2 $\pm$ 1.2 Ma and an Ar age of 105.3 $\pm$ 1.3 Ma. The Hongliuxia volcanic fields to the NE of the Changma Basin produces a K age of 116.6 $\pm$ 2.2 Ma and an Ar age of 112 $\pm$ 0.6 Ma. The Jianquanzi locality south of the Changma Basin produces a K age of 112.8 $\pm$ 3.4 Ma and an Ar age of 118.8 $\pm$ 3.6 Ma. Zeng *et al.* (2006) report cross-cutting dykes from the Hongliuxia volcanic field dated as *c.* 85 Ma. The combined biostratigraphic and numerical age data suggest that the Changma Basin began accumulating sediment no older than Hauterivian (based on pollen records), is older than the Coniacian (based on the cross-cutting dykes), but is likely Barremian to Aptian based on the similarities to the Jehol biota.

Methods

The Xiagou Formation in this location consists primarily of greyish-yellowish shales, siltstones, calcareous shales, argillaceous limestones and sandstones deposited in fluvio-lacustrine environments. Significant structural deformation has occurred in this region such that the Xiagou Formation occurs at very high dip angles to almost vertically oriented beds. Samples from two sections were collected at *c.* 1 m intervals. One of the sections is from an active fossil bird quarry that has produced numerous specimens of *G. yumenensis*, a primitive ornithuran aquatic bird. The other section is from an inactive quarry that produced the first specimens of *G. yumenensis*. The two sites are located on either side of a dirt road *c.* 100 m apart, with the inactive quarry down-section of the active quarry (Fig. 1). Correlation of the two sections is tenuous, because the two sections are primarily laminated shales that are vertically oriented. In addition, small lateral faults and covered sections make direct correlation difficult. The section from the active quarry was 53.19 m thick, with a total of 64 samples collected. The section from the inactive quarry was 41 m thick, with a total of 40 samples collected.

Approximately 1–2 g of each hand sample was powdered using a hand-held drill and dried for 24 h in an oven. Approximately 1 g of each sample was decarbonated using 0.5 M HCl for 24 h or until all carbonate was removed. After decarbonation, the remaining HCl was decanted and samples were rinsed with deionized-distilled water until the supernatant reached neutrality. Samples were dried in an oven at 45 °C for 24–48 h and re-homogenized with a mortar and pestle. Approximately 0.3–2 mg per sample was combusted with a Costech elemental analyser, with the resulting CO_2 analysed with a ThermoFinnigan MAT 253 continuous-flow isotope ratio mass spectrometer. The analysis resulted in $\delta^{13}C$ values for both bulk sedimentary organic carbon and total organic carbon (TOC). Aliquots of samples that were not decarbonated were analysed for stable isotopic compositions of carbonate oxygen and carbon. Another set of microsampled carbonates were drilled from polished slabs of hand samples. The carbonates (*c.* 50 μg) were reacted with 100% phosphoric acid in a KIEL III carbonate device connected to a ThermoFinnigan MAT 253 dual-inlet isotope ratio mass spectrometer. All analyses were

carried out at the Keck Palaeoenvironmental and Environmental Stable Isotope Lab at the University of Kansas. All samples are reported relative to V-PDB, with accuracy monitored by analysis of international standards such as NBS-19 and NBS-18 (for carbonates) and IAEA-600 and USGS 24 (for organic carbon) to within 0.1‰.

Results

Sedimentary organic carbon isotope curve

The carbon isotope curve of organic matter has an overall shift to heavier $\delta^{13}C$ values up-section for both the active quarry section and the inactive quarry section (Fig. 2; Table 1). The $\delta^{13}C_{org}$ in the first 7 m of the active quarry varies at the base of the section by more than 5‰. It begins with an overall decrease in $\delta^{13}C_{org}$ from −25.0‰ to −31.8‰ (0 to 7 m), the most negative value for the section. This is followed by a sharp peak characterized by an *c.* 5‰ increase to −25.3‰ followed by a decrease back to −31.0‰, at 10.3 m. There is a pronounced increase in $\delta^{13}C_{org}$ of *c.* 6‰ to −25‰ from 10.3 to 17.5 m. The $\delta^{13}C_{org}$ curve then oscillates by *c.* 2–3‰, before a sharp peak occurs at −21.5‰ (38.18 m), followed by a decrease to −27.2‰ at 41.74 m. The $\delta^{13}C_{org}$ finally increases to −20.9‰ at 45.74 m, the most enriched value of the section. The top of the section (45.74–52.74 m) is characterized by a decrease in $\delta^{13}C_{org}$ of *c.* 3‰.

The inactive quarry samples includes the lowest $\delta^{13}C_{org}$ value of both sections (−33.2‰); this occurs 1 m above the base of the section. The $\delta^{13}C_{org}$ curve fluctuates by *c.* 3–5‰, over 12 m, but gradually increases to a value of −26.5‰ at 12 m. The curve again oscillates by *c.* 2‰ between 12 and 19 m before increasing to −22.9‰ at 21 m, and then decreases significantly to −28.7‰ at 25 m. A large shift to more positive values for $\delta^{13}C_{org}$ occurs above 25m, and values increase to −22.7‰ at 27.33 m, followed by a smaller positive step at 31 m to −20.7‰ (the most positive value for this section), with an overall increase of 8‰ between 25 and 31 m. The $\delta^{13}C_{org}$ curve decreases again to −27.6‰ at 34 m, before it increases to a second positive peak of −21.6‰ at 39 m.

Carbonate carbon isotope curve

The $\delta^{13}C_{carb}$ curve for the active quarry section shows an initial decrease in $\delta^{13}C$ from 9.6‰ at 1 m to 3.7‰ at 5 m. The $\delta^{13}C_{carb}$ then increases to a maximum value of 11.4‰ at 8.5 m (Fig. 3a, Table 1). The curve varies by *c.* ±1‰, with an overall decrease in $\delta^{13}C_{carb}$ from the maximum of 11.4‰ to 9.5‰ over a thickness of 24.6 m, followed by a 7.8‰ decrease to 1.7‰ at 34.1 m. The carbon isotope curve then fluctuates significantly over the next 19 m by 8‰ with a maximum value of 8.4‰ at 35.6 m, and a minimum value of 0.4‰ at 38.9 m.

The $\delta^{13}C_{carb}$ in the inactive quarry increases from the base of the section at 7.0‰ to 10.2‰ at

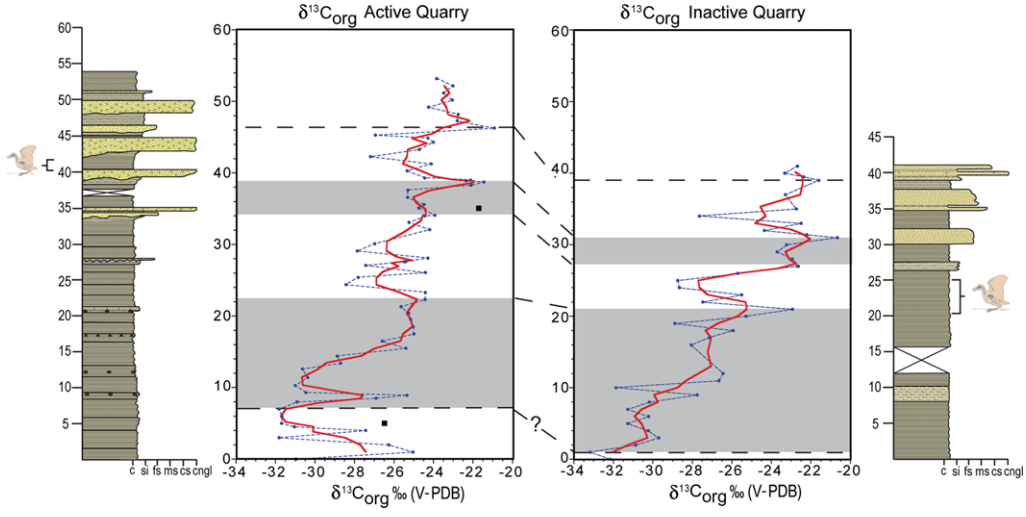

Fig. 2. Lithostratigraphy and bulk sedimentary organic carbon stable isotope chemostratigraphy from the active and inactive bird quarries. The solid red lines reflect a three-point running average of data depicted by thin, blue dashed lines. The square data points in the active quarry section are values for charcoalified wood. The two sections are correlated based on the four segments depicted as alternating shaded/non-shaded segments. Profile is in metres. Horizontal scale indicated grain size: c, clay; si, silt; fs, fine sand; ms, medium sand; cs, coarse sand; cngl, conglomerate.

Table 1. *Chemostratigraphic data*

Section	Sample	Metres	$\delta^{13}C_{org}$ ‰ (V-PDB)	$\delta^{13}C_{carb}$ ‰ (V-PDB)	$\delta^{18}O_{carb}$ ‰ (V-PDB)	TOC (%)
Active quarry	CBBQ-1	0.00	−31.0	7.3	−0.1	2.6
	CBBQ-2	1.00	−25.0	9.6	−5.5	0.4
	CBBQ-3	2.00	−26.3			0.4
	CBBQ-4	3.00	−31.8	3.7	−6.7	1.0
	CBBQ-5	4.00	−27.4	7.4	−8.9	0.1
	CBBQ-6aux	4.50	−31.1	5.0	−8.3	6.5
	CBBQ-6	5.00	−31.7	3.7	−7.5	1.7
	CBBQ-6 charcoal	5.00	−26.5			
	CBBQ-7	6.00	−31.7	9.2	−7.1	0.0
	CBBQ-8r	7.00	−31.8	11.3	−1.6	3.8
	CBBQ-9	8.00	−30.9	6.9	−8.6	0.8
	CBBQ-10	8.50	−26.9	11.4	−0.5	0.3
	CBBQ-11	8.90	−25.3			0.4
	CBBQ-12r	9.30	−30.5			5.7
	CBBQ-13r	10.30	−31.0	9.5	−0.2	2.5
	CBBQ-14r	11.40	−30.4	9.0	0.7	2.5
	CBBQ-15r	12.60	−30.6	8.3	−2.0	3.2
	CBBQ-16	13.40	−28.7	9.2	−1.3	0.9
	CBBQ-17	14.40	−28.9	9.0	−4.0	0.9
	CBBQ-18	15.50	−25.4	10.5	0.1	0.5
	CBBQ-19	16.50	−26.6	8.6	−1.2	0.2
	CBBQ-20	17.50	−25.0			0.2
	CBBQ-21	18.50	−25.0	8.5	−4.3	0.4
	CBBQ-22	19.55	−25.2	7.4	−1.3	0.2
	CBBQ-23	20.40	−25.3	6.9	−6.3	0.4
	CBBQ-24	21.30	−25.6	8.1	−2.4	0.2
	CBBQ-25	22.30	−24.4	10.5	−2.4	0.2
	CBBQ-26	23.30	−24.4	9.7	−1.6	0.4
	CBBQ-27	24.40	−28.4	8.1	−1.2	1.5
	CBBQ-28	25.40	−27.8	8.0	−3.5	1.3
	CBBQ-29	26.10	−24.4	9.0	−4.9	0.4
	CBBQ-30	27.10	−27.4	7.8	−5.6	1.2
	CBBQ-31bottom	27.60	−25.5	6.2	−6.7	0.3
	CBBQ-31top	27.60	−25.4	8.3	−4.3	0.4
	CBBQ-32	28.10	−24.3	10.5	−3.2	0.2
	CBBQ-33	29.10	−27.9			3.7
	CBBQ-34	30.10	−27.0	7.2	−4.5	0.6
	CBBQ-36	32.10	−24.2			0.2
	CBBQ-37	33.10	−25.2	9.5	−5.4	0.1
	CBBQ-38shale	34.00	−24.4	3.7	−6.5	0.7
	CBBQ-38ss	34.10	−23.9	1.7	−10.0	0.1
	CBBQ-39	35.10	−24.8	3.8	−12.9	0.1
	CBBQ-39 charcoal	35.10	−21.7			
	CBBQ-40	35.60	−24.5	8.4	−4.0	0.5
	CBBQ-41	36.60	−25.3			1.0
	CBBQ-42	37.60	−25.3	7.9	−4.5	0.5
	CBBQ-43	38.29	−22.1	4.2	−13.0	1.1
	CBBQ-43bR	38.72	−21.4			1.4
	CBBQ-43c	38.89	−22.3	0.4	−11.7	4.6
	CBBQ-43dR	38.99	−22.1	1.7	−12.1	2.3
	CBBQ-44	39.29	−24.4			0.1
	CBBQ-45	40.29	−25.3			0.1
	CBBQ-46	41.29	−24.1	3.5	−9.3	0.5
	CBBQ-47	42.29	−27.2	8.0	−4.0	1.6
	CBBQ-48	43.29	−24.7			0.1

(*Continued*)

Table 1. *Continued*

Section	Sample	Metres	$\delta^{13}C_{org}$ ‰ (V-PDB)	$\delta^{13}C_{carb}$ ‰ (V-PDB)	$\delta^{18}O_{carb}$ ‰ (V-PDB)	TOC (%)
	CBBQ-49b	44.29	−24.0			0.2
	CBBQ-49.5	44.89	−24.3	2.9	−13.2	0.5
	CBBQ-50	45.29	−26.9			0.1
	CBBQ-51	46.29	−20.9			0.4
	CBBQ-52	47.29	−22.8			1.6
	CBBQ-53	48.19	−22.8	2.3	−12.2	6.5
	CBBQ-54	49.19	−24.3			0.1
	CBBQ-55	50.19	−23.1			1.3
	CBBQ-56	51.19	−23.5			1.1
	CBBQ-57	52.19	−23.0	2.6	−8.0	0.8
	CBBQ-58	53.19	−23.8	4.1	−7.8	0.6
Inactive quarry	CB-G-1	0.00	−32.2			3.5
	CB-G-2	1.00	−33.2	7.0	−9.9	4.0
	CB-G-3	2.00	−30.9			4.4
	CB-G-4	3.00	−29.7	10.2	−4.9	2.7
	CB-G-5	4.00	−30.2	8.8	−1.4	1.6
	CB-G-6	5.00	−31.3			3.9
	CB-G-7	6.00	−30.2			8.2
	CB-G-8	7.00	−31.3	9.2	−0.1	2.8
	CB-G-9	8.00	−30.2	8.3	−0.1	1.5
	CB-G-10	9.00	−27.8	8.1	−7.1	0.5
	CB-G-11	10.00	−31.9	7.9	−1.8	2.9
	CB-G-12	11.00	−26.7	8.4	−3.3	15.8
	CB-G-13	12.00	−26.4	9.5	−0.7	0.6
	CB-G-14	16.00	−28.1			3.5
	CB-G-15	17.00	−27.2	9.9	−2.9	2.6
	CB-G-16	18.00	−25.9	6.7	−3.7	1.5
	CB-G-17	19.00	−28.9			3.9
	CB-G-18r	20.00	−25.3	7.0	−6.2	0.8
	CB-G-19r	21.00	−22.9			1.0
	CB-G-20	22.00	−27.5	3.9	−6.8	3.4
	CB-G-21r	23.00	−25.5	7.5	−1.2	0.6
	CB-G-22	24.00	−28.7	6.5	−5.0	2.9
	CB-G-23	25.00	−28.7	8.4	−7.6	1.3
	CB-G-24	26.00	−25.7	8.3	−4.2	0.9
	CB-G-25black shale	26.99	−22.7	4.1	−6.5	0.9
	CB-G-25r	27.00	−22.6	4.0	−6.4	0.5
	CB-G-26r	28.00	−22.9	7.0	−5.7	0.5
	CB-G-27r	29.00	−23.7	9.5	−2.2	0.6
	CB-G-28	30.00	−23.2	5.6	−5.2	0.9
	CB-G-29	31.00	−20.7			0.2
	CB-G-30	31.40	−22.2			0.1
	CB-G-31	32.00	−24.4	2.4	−9.4	0.1
	CB-G-32	33.00	−22.5	3.8	−7.5	0.5
	CB-G-33	34.00	−27.6	7.1	−8.0	1.3
	CB-G-34	35.00	−22.7			1.0
	CB-G-36	37.00	−23.3	2.6	−12.9	0.1
	CB-G-37	39.00	−21.6	4.1	−12.8	0.2
	CB-G-38	39.49	−22.4			1.3
	CB-G-39	40.00	−23.3			0.0
	CB-G-40	41.00	−22.7	4.8	−13.7	0.1

3 m (Fig. 3a). The curve oscillates slightly before decreasing to a $\delta^{13}C_{carb}$ value of 3.9‰ at 22 m. The curve then begins a series of large fluctuations of *c.* 8‰ over the next 19 m with a maximum value of 9.5‰ at 29 m and a minimum value of 2.4‰ at 32 m.

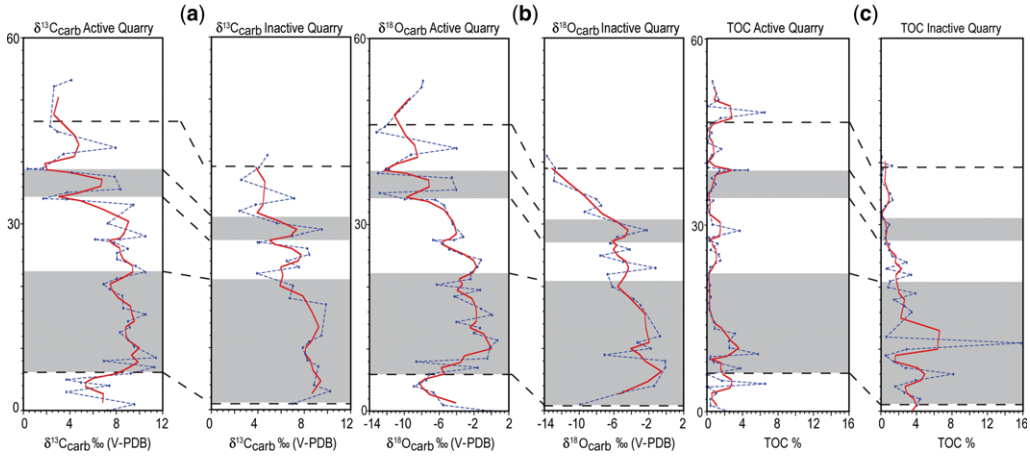

Fig. 3. Chemostratigraphic profiles for (**a**) $\delta^{13}C$ of carbonate, (**b**) $\delta^{18}O$ of carbonate and (**c**) TOC. Shaded segments are defined based on the bulk sedimentary organic carbon $\delta^{13}C$ chemostratigraphic profile.

Carbonate oxygen isotope curve

The $\delta^{18}O$ curve of the active quarry section decreases from −0.1‰ at the base of the section to a value of −9.0‰ at 4 m, then increases to a maximum value of 0.7‰ at 11.4 m (Fig. 3b, Table 1). This initial increase is followed by a decrease to −12.8‰ at 35.1 m. Superimposed on this decrease are higher frequency fluctuations of *c.* 4‰. Over the next 18 m, the curve begins a series of large fluctuations with a range of *c.* 9‰.

The $\delta^{18}O$ curve of the inactive quarry section increases from −9.9‰ at 1 m to a maximum value of −0.1‰ at 7 m, before beginning a general decrease in $\delta^{18}O$ (Fig. 3b). The decrease is marked by three negative peaks of −7.1‰, −6.8‰ and −7.6‰ at 9, 22 and 25 m, respectively. The $\delta^{18}O$ curve then increases to −2.2‰ at 29 m before beginning a steady decrease in composition to −13.7‰ at the top of the section (41 m).

Total organic matter curve

The TOC curves for both sections are variable (Fig. 3c, Table 1). The active quarry section varies between 0.04% and 6.6%. The TOC concentrations are generally below 1%, but several increases in TOC occur at 4.5 m (6.6%), 7m (3.8%), 9.3 m (5.8%), 29.1 m (3.7%), 38.89 m (4.6%) and 48.19 m (6.5%). The inactive quarry section has greater TOC values, which increase from 3.5% at the base of the section to 15.8% at 11 m. The TOC steadily decreases to values that are generally less than 1% from 25 m to the top of the section.

Carbon and oxygen isotope cross-plots

Cross-plots of microsampled micritic lamina and beds from seven hand samples in the active quarry and six hand samples from the inactive quarry show an overall covariation of $\delta^{13}C$ and $\delta^{18}O$ (Fig. 4; Table 2). The $\delta^{18}O$ values from the active quarry range from −7.3‰ to 1.2‰ and average −3.5‰. The $\delta^{13}C$ values from the active quarry range from 6.0‰ to 10.9‰ and average 8.2‰. The $\delta^{18}O$ values from the inactive quarry range from −7.7‰ to −0.1‰ and average −3.6‰. The $\delta^{13}C$ values from the inactive quarry range from 6.5‰ to 10.7‰ and average 8.4‰.

Interpretation

Local correlation

The two sections are correlated based on the overall increase in $\delta^{13}C_{org}$. The overall increase of *c.* 7.5‰ in the three-point running-mean curve (thick red line in Fig. 2) of the data is the lowest segment that is correlated. The lowest portion of this correlation is tenuous because the distinct decrease in $\delta^{13}C$ composition in the first 10 m of the active quarry is not present in the shorter inactive quarry. The prominent positive peak at −25.3‰ in the active quarry section is recognized, but is not as prominent in the inactive quarry (Fig. 2). The next segment that is correlated between the two sections is a negative excursion, which in both three-point running means reaches a point of *c.* −27‰. The uppermost segments that are correlated are the two

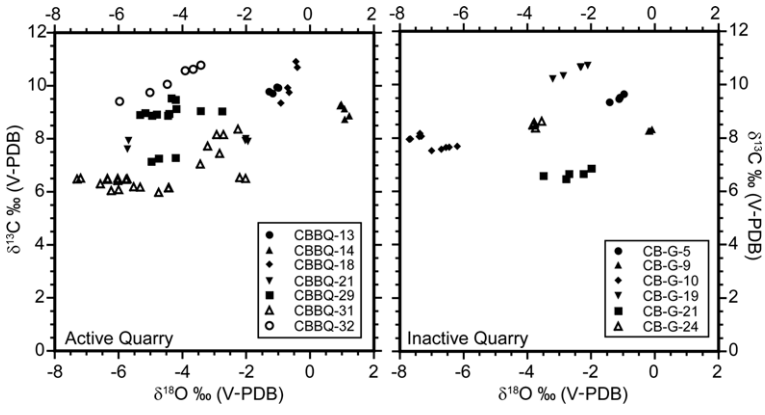

Fig. 4. Cross-plot of carbon and oxygen isotopic composition of microsampled carbonates from hand samples from the active and inactive quarry sections.

prominent positive excursions of *c.* −22‰ in the three-point running-mean curve.

To test the validity of the $\delta^{13}C_{org}$ correlation between the two sections, stratification of the carbon isotope defined segments described above can be applied to the carbonate $\delta^{13}C$ and $\delta^{18}O$ curves (Fig. 3a, b). The segments produce a good correlation with the $\delta^{13}C_{carb}$ curve, with an increase in values to 11.4‰ in the active quarry and 10.23‰ in the inactive quarry. This is followed by an overall plateau and shallow decrease up-section in $\delta^{13}C_{carb}$ values. The second segment is characterized by an overall increase and decrease in $\delta^{13}C$ to as low as 1.7‰ in the active quarry, but higher in the inactive quarry (4.0‰). The third and fourth segments each correspond, with positive excursions in the $\delta^{13}C_{carb}$ curve. The $\delta^{18}O$ record is also consistent with the correlation based on the $\delta^{13}C_{org}$ curve. Both the inactive and active $\delta^{18}O$ curves increase significantly from *c.* −9‰ to as high as 0.69‰ in the active quarry (−0.10‰ in the inactive quarry), then shallowly decrease. The second segment is characterized by a slight increase but overall continuation of decreasing $\delta^{18}O$ values. The third and fourth segments are also characterized by positive excursion, but an overall pattern of decreasing $\delta^{18}O$ values. It should be noted that the lightest $\delta^{18}O$ values are consistently, although not exclusively, from sandstones. This could indicate that the carbonate cement was influenced by lighter $\delta^{18}O$ water, possibly sourced from rivers draining upland areas and precipitating as early cements with lower isotopic compositions, or that the coarser rocks in the upper part of the sections have been influenced by later diagenetic fluids and cements. A comparison of the TOC record shows a poor correlation that is probably due to the fact that the TOC varies spatially throughout the section (Fig. 3c). In hand samples, this is evident visually as concentrations of dark organic material, primarily plant fragments. The chemostratigraphic correlation places the inactive quarry *c.* 10–15 m lower than the active quarry, suggesting more than one accumulation of fossilized bird remains.

Palaeolimnological interpretation

Lacustrine carbonates are generally precipitated chemically and/or are microbially mediated. Aquatic plants also contribute by reducing the pH of lacustrine system when consuming CO_2. The carbonates sampled at the Changma bird quarries consist of micritic lamina, small (centimetre scale or smaller) thrombolitic masses, or massive centimeter-scale beds. The $\delta^{13}C$ of carbonates is controlled by the $\delta^{13}C$ composition of dissolved inorganic carbon (DIC), which responds not only to the $\delta^{13}C$ of atmospheric CO_2, but also to processes within the lake that affect the DIC, such as an accelerated biological pump drawing light carbon from the reservoir or degassing of gases such as methane. The overall enriched compositions of the $\delta^{13}C_{carb}$ values (as high as 11‰) suggest that methanogenesis and ebullition of isotopically light methane may have caused this enrichment (Talbot & Kelts 1986). A similar effect has been suggested for the lacustrine Yixian Formation, which also contains well-preserved birds and other fossils (Ludvigson *et al.* 2005).

Covariant trends in the carbon and oxygen cross-plots indicate an overall evaporative and closed lake system (Fig. 4). The lowest $\delta^{18}O$ carbonate values (*c.* −7.5‰) probably reflect the average precipitation composition within the catchment area of

Table 2. *Microsampled carbonates*

Section	Sample	$\delta^{18}O$ ‰ (V-PDB)	$\delta^{13}C$ ‰ (V-PDB)	Section	Sample	$\delta^{18}O$ ‰ (V-PDB)	$\delta^{13}C$ ‰ (V-PDB)
Active quarry	CBBQ-13.1	−1.17	9.71		CBBQ-31.16	−5.77	6.47
					CBBQ-31.17	−5.53	6.19
	CBBQ-13.2	−1.00	9.92		CBBQ-13.18	−5.32	6.18
	CBBQ-13.3	−1.28	9.78		CBBQ-31.19	−4.42	6.16
	CBBQ-13.5	−1.03	9.95		CBBQ-31.20	−4.74	5.98
	CBBQ-14.1	0.94	9.25		CBBQ-31.21	−4.44	6.15
	CBBQ-14.2	0.98	9.30		CBBQ-31.22	−3.21	7.72
	CBBQ-14.3	1.23	8.87		CBBQ-31.24	−2.71	8.16
	CBBQ-14.4	1.09	8.74		CBBQ-31.25	−2.93	8.16
	CBBQ-14.5	1.08	9.13		CBBQ-32.2	−3.42	10.78
	CBBQ-18.1	−0.91	9.35		CBBQ-32.3	−3.91	10.57
	CBBQ-18.2	−0.66	9.74		CBBQ-32.4	−4.48	10.06
	CBBQ-18.3	−0.44	10.91		CBBQ-32.5	−3.66	10.62
	CBBQ-18.4	−0.40	10.69		CBBQ-32.6	−5.97	9.41
	CBBQ-18.5	−0.70	9.92		CBBQ-32.8	−5.02	9.75
	CBBQ-21.1	−2.03	7.94	Inactive quarry	CB-G-5.1	−0.97	9.65
	CBBQ-21.2	−1.95	7.90				
	CBBQ-21.3	−2.01	8.00		CB-G-5.2	−1.42	9.34
	CBBQ-21.4	−5.68	7.94		CB-G-5.4	−1.10	9.52
	CBBQ-21.5	−5.72	7.61		CB-G-5.5	−1.13	9.46
	CBBQ-29.2	−4.42	8.94		CB-G-9.1	−0.09	8.32
	CBBQ-29.3	−4.46	8.88		CB-G-9.2	−0.19	8.26
	CBBQ-29.4	−2.76	9.05		CB-G-9.4	−0.16	8.26
	CBBQ-29.5	−3.43	9.06		CB-G-9.5	−0.08	8.32
	CBBQ-29.6	−5.33	8.91		CB-G-10.1	−6.70	7.58
	CBBQ-29.7	−5.17	8.98		CB-G-10.2	−7.00	7.52
	CBBQ-29.8	−4.81	8.92		CB-G-10.3	−6.45	7.66
	CBBQ-29.9	−4.96	8.88		CB-G-10.4	−6.20	7.69
	CBBQ-29.10	−4.22	9.48		CB-G-10.5	−6.55	7.64
	CBBQ-29.11	−4.35	9.54		CB-G-10.6	−7.33	8.06
	CBBQ-29.12	−4.20	9.13		CB-G-10.7	−7.37	8.17
	CBBQ-29.13	−4.97	7.15		CB-G-10.8	−7.39	8.05
	CBBQ-29.14	−4.22	7.29		CB-G-10.9	−7.67	7.96
	CBBQ-29.15	−4.74	7.27		CB-G-10.10	−7.70	7.95
	CBBQ-31.1	−2.83	7.45		CB-G-19.1	−2.34	10.66
	CBBQ-31.2	−2.21	6.53		CB-G-19.2	−2.87	10.33
	CBBQ-31.3	−2.02	6.50		CB-G-19.3	−2.31	10.67
	CBBQ-31.4	−3.44	7.04		CB-G-19.4	−2.10	10.72
	CBBQ-31.5	−2.26	8.37		CB-G-19.5	−3.20	10.21
	CBBQ-31.6	−6.57	6.30		CB-G-21.2	−1.99	6.86
	CBBQ-31.7	−6.02	6.50		CB-G-21.3	−2.24	6.66
	CBBQ-31.8	−6.02	6.42		CB-G-21.4	−3.50	6.59
	CBBQ-31.9	−6.34	6.47		CB-G-21.5	−2.69	6.66
	CBBQ-31.10	−7.30	6.48		CB-G-21.6	−2.79	6.46
	CBBQ-31.11	−7.19	6.51		CB-G-24.1	−3.79	8.54
	CBBQ-31.12	−6.35	6.50		CB-G-24.2	−3.78	8.57
	CBBQ-31.13	−6.23	6.05		CB-G-24.3	−3.55	8.63
	CBBQ-31.14	−6.00	6.08		CB-G-24.4	−3.75	8.37
	CBBQ-31.15	−5.73	6.49		CB-G-24.5	−3.83	8.48

the lake, while the highest $\delta^{18}O$ values indicate evaporative enrichment (Talbot 1990). Increased evaporative conditions may have contributed to carbon isotopic enrichment up-section. A closed lake is consistent with the overall tectonic setting, which produced numerous intermontane basins.

Global correlation

Over the past decade, numerous high-resolution carbon isotope curves from Cretaceous marine sections have been correlated based on their record of positive and negative excursions (Menegatti

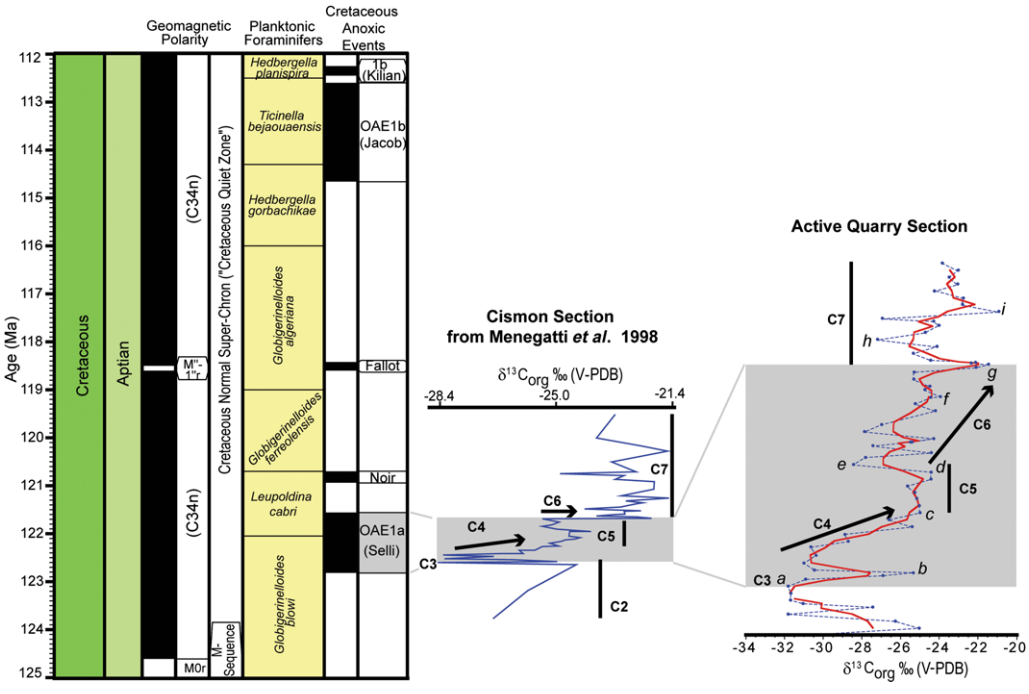

Fig. 5. Correlation of the active quarry section to the Cismon section, Italy, from Menegatti *et al.* (1998). The negative excursion at C3 followed by the two-step positive excursion defined by C4, C5 and C6 define the 'Selli Equivalent' associated with ocean anoxic event 1a (OAE 1a) (shaded region). The age, chronostratigraphy, magnetostratigraphy, planktonic foraminiferal biozones, and anoxic event record were created using the Time Scale Creator version 4.2.5 software (TSCreator 2011).

et al. 1998; Erba *et al.* 1999; Price 2003; and others). The largest change in $\delta^{13}C$ compositions occurs over the Early Aptian C3 to C7 segments defined by Menegatti *et al.* (1998), in which marine $\delta^{13}C_{carb}$ varies from slightly less than 1.6‰ to slightly greater than 4.4‰ in the classic Cismon section from the Italian Alps. The $\delta^{13}C_{org}$ record from the Changma bird quarries shows an even greater change in $\delta^{13}C$, with a *c.* 7‰ increase from −28.4‰ to −21.2‰. This negative excursion followed by very large positive excursion is also observed in terrestrial $\delta^{13}C_{org}$ records in wood from England and Japan (Grocke *et al.* 1999; Ando *et al.* 2002). It is the C3 to C7 segments of the global $\delta^{13}C$ record to which we correlate the Xiagou Formation lacustrine $\delta^{13}C$ record (Fig. 5).

The minimum $\delta^{13}C_{org}$ value in the Xiagou Formation curves (Figs 2 & 5) is identified as the C3 negative excursion. The initial 7‰ increase in $\delta^{13}C_{org}$ (Figs 2 & 5) is identified as C4, the first of two positive isotope shifts. The C5 segment in European marine sections is defined by uniform $\delta^{13}C$ values, although both curves in Menegatti *et al.* (1998) and Erba *et al.* (1999) show a slight decrease in $\delta^{13}C$, and Price (2003) and Ando *et al.* (2008) also show a somewhat more significant decrease in $\delta^{13}C$. C5 is identified in the active and inactive quarry sections as the segment after the initial increase in carbon isotopic composition, to the most negative point within the non-shaded segment of Figure 2 (see also Fig. 4). In the active quarry section this segment is characterized by nearly stable $\delta^{13}C$ values with a decrease of *c.* 4‰. In the inactive quarry section, this segment is less well defined and has slightly greater $\delta^{13}C$ fluctuations. The second major positive excursion (C6) is identified by the 7–8‰ increase in $\delta^{13}C_{org}$ from the negative point in the non-shaded section of Figure 2 to the positive excursion defining the upper boundary of the second shaded segment in Figure 2 (see also Fig. 4). The uppermost sections of the carbon isotope curves are identified as the start of the C7 segment.

The overall increase in $\delta^{13}C_{org}$ from C3 to the maximum value in C7 is as much as 12.5‰ in the inactive quarry and 10.9‰ in the active quarry, which is an extremely large change in carbon isotope composition. Other terrestrial organic matter records show similar magnitudes in $\delta^{13}C$ shifts. Heimhofer *et al.* (2003) shows an 8.5‰ change in

carbon isotope composition of terrestrial organic matter from Portugal. Moreover, Grocke *et al.* (1999) shows a *c.* 11‰ change from the lightest to heaviest $\delta^{13}C$ composition of wood from the Early Cretaceous Isle of Wight. This enhanced magnitude effect may be a result of a more buffered ocean system due to a larger carbon reservoir, whereas the terrestrial carbon reservoir may be more sensitive to variations in atmospheric $\delta^{13}C$ changes. This effect can also be attributed at least in part to changes in $\delta^{13}C$ plant composition due to changes in pCO_2, with increasing pCO_2 causing lighter plant composition, and decreasing pCO_2 causing heavier plant compositions (van de Water *et al.* 1994; Körner *et al.* 1988; Grocke *et al.* 1999). Partitioning between organic carbon and DIC within the lacustrine setting may also cause a large separation between $\delta^{13}C_{org}$ and $\delta^{13}C_{carb}$, in which high productivity and enhanced burial of light carbon can cause significant enrichment in the remaining DIC, and thus $\delta^{13}C_{carb}$ (Leng *et al.* 2006). Hollander & McKenzie (1991) also show enrichment in particulate organic carbon (POC) $\delta^{13}C$ during seasonal highs in productivity. These processes could account for the large variation in $\delta^{13}C_{org}$.

We consider whether these changes in fractionation between DIC and POC are the origins of the overall stratigraphic $\delta^{13}C_{org}$ pattern. As mentioned above, this process could account for the difference in magnitude of the $\delta^{13}C_{org}$ variation, but it is not likely to be the sole cause of the pattern observed stratigraphically. There are four reasons for this. First, the variations as described by Hollander & McKenzie (1991) and Leng *et al.* (2006) often occur as seasonal variations. The large-scale stratigraphic pattern that we correlate with global changes in CO_2 occurs at much longer timescales than these seasonal changes. Second, if the increase in $\delta^{13}C_{org}$ were solely the result of high productivity, TOC and $\delta^{13}C$ would be positively correlated. Figure 6 shows no correlation between these two variables. Third, two pieces of charcoalified wood were analysed from within the active quarry section: one near the base of the section at 5 m (−26.5‰) and another at 35.1 m (−21.7‰) – an increase of 4.8‰ (square data points in Fig. 2). Both values are somewhat heavier than the bulk organic carbon isotopic composition, which may be due to the fact that coalified and charcoalified plant remains often become more enriched than their original isotopic composition (Robinson & Hesselbo 2004). While any conclusions drawn from only two data points from charcoalified wood are somewhat uncertain, it is consistent with changing isotopic compositions of atmospheric CO_2 as a primary control on the isotopic composition of both bulk organic carbon and wood carbon. Finally, we consider whether an increase in terrestrial organic matter (with slightly heavier isotopic composition) is the cause of the increase in $\delta^{13}C$ for bulk organic matter. It is possible that the coarsening-upward section signals a greater amount of terrestrial input over aquatic organic matter; however, this is an unlikely primary cause for the change in carbon isotopic composition, because the increase in $\delta^{13}C_{org}$ occurs well below (*c.* 10 m or more) the first occurrence of sandstone in both the inactive and active quarry sections.

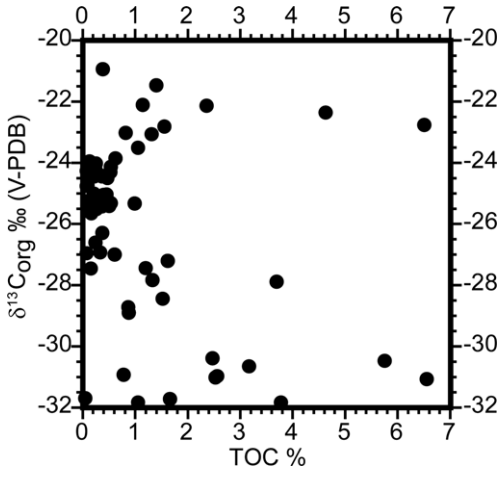

Fig. 6. Carbon isotopic composition of bulk sedimentary organic carbon of the active quarry, plotted v. total organic carbon. No correlation between the two variables is recognized.

Implications

Assignment of the Xiagou Formation to the C3 to C7 segments firmly places the age of the bird quarries in the early Aptian Age. Menegatti *et al.* (1998) defined the 'Selli Equivalent', which is associated with oceanic anoxic event 1a (OAE1a), as the increase in $\delta^{13}C$ (C4), stabilized $\delta^{13}C$ of C5, followed by the increase (C6) of $\delta^{13}C$ values to maximum early Aptian Age values. Based on the APTICORE reference core from Cismon, this interval is almost entirely within the *Leupoldina cabri* planktonic foraminiferal biozone, which occurs just above the magnetic polarity zone CM0 (Erba *et al.* 1999). In many other pelagic marine sections, the first occurrence of *L. cabri* occurs later than at the Cismon section, so the sequence is also correlative to the upper part of the *Globigerinoides blowii* biozone (Fig. 4). Regardless of the placement of the boundary between these two biozones, we can narrow down the age of the lacustrine Xiagou Formation strata in the Changma Basin to between 124 and 120 Ma (Gradstein *et al.* 2004; Ogg *et al.* 2008).

Many authors have concluded that the negative and subsequent positive carbon isotope excursion indicates dramatic changes in palaeoclimate during the Aptian, and the early Aptian Age is thought to be the initiation of the mid-Cretaceous greenhouse period (Menegatti *et al.* 1998; Grocke *et al.* 1999; Jahren *et al.* 2001; van Breugel *et al.* 2007; Ando *et al.* 2008). The light carbon signature has been attributed to an increase in volcanic activity (i.e. at the Ontong Java Plateau, with a release of isotopically light carbon into the atmosphere) (Menegatti *et al.* 1998). The abruptness and strong depletion at C3 have also been attributed to a release of extremely isotopically light carbon from methane into the atmosphere (e.g. Grocke *et al.* 1999; Jahren *et al.* 2001; van Breugel *et al.* 2007; Ando *et al.* 2008). According to this hypothesis, the release of greenhouse gases (methane and carbon dioxide) would result in increased global temperatures and greater weathering, increasing nutrient supply into the oceans. This would have increased primary productivity and anoxic conditions as organic carbon burial increased (resulting in widespread black shale deposition). As organic carbon burial increased, the remaining pool of carbon in the ocean, and hence atmospheric CO_2 in equilibrium with the ocean, increased in isotopic composition. Subsequent drawdown of CO_2 due to carbon burial would have caused global cooling (Jenkyns 2003; Weissert & Erba 2004; Ando *et al.* 2008; Strohmenger *et al.* 2010). Changes in marine fauna (ex. rudist extinctions) during this time are thought to have been triggered by these dramatic shifts in climate; whether there is evidence for changes in continental flora and fauna remains to be seen. Identification of this interval in Early Cretaceous strata of NW China will allow examination of the impact of this event on terrestrial flora and fauna.

Conclusions

Carbon isotope chemostratigraphy can significantly aid the correlation of continental strata. The $\delta^{13}C_{org}$ curves of two profiles within lacustrine strata of the Xiagou Formation are characterized by a negative excursion followed by a large increase in $\delta^{13}C$ of *c.* 12.5‰. Chemostratigraphic profiles of $\delta^{13}C_{org}$, $\delta^{13}C_{carb}$ and $\delta^{18}O_{carb}$ from the two sections places the inactive fossil bird quarry *c.* 10–15 m below the active quarry. The negative excursion in the $\delta^{13}C_{org}$ curve corresponds with the global C3 negative excursion of Menegatti *et al.* (1998), and the subsequent increase in $\delta^{13}C$ corresponds to the C4 through C6 segments. This correlation firmly places this section of the Xiagou Formation within the early Aptian (124–120 Ma) Stage (Gradstein *et al.* 2004; Ogg *et al.* 2008). The identification of these carbon isotope excursions indicates that the Xinminpu Group encompasses the onset of potential greenhouse conditions represented by the C3 negative excursion, followed by subsequent cooling, represented by the increase in $\delta^{13}C$.

The authors wish to thank the members of the Summer 2006 Sino-KU expedition (J. J. Smith, B. F. Platt, C. A. Suarez, B. Totten, and E. Tremain). G. Cane (KPESIL) was instrumental in sample analyses. Funding was provided by an NSF supplemental award EAR-0636207 travel grant from the Office of International Programs of KU Research and Graduate Studies office to L. González and G. Ludvigson, and an AAPG Grants-in-Aid to M. Suarez. Funding was also provided by the National Natural Science Foundation of China (40672007 and 41072019) to Hai-Lu You. We are grateful to the crew of the former Fossil Research and Development Center of the Third Geology and Mineral Resources Exploration Academy of Gansu Province for field work assistance. This manuscript was improved greatly by constructive comments and suggestions from one anonymous reviewer and F. Neubauer.

References

Ando, A., Kakegawa, T., Takashima, R. & Saito, T. 2002. New perspective on Aptian carbon isotope stratigraphy: data from $\delta^{13}C$ records of terrestrial organic matter. *Geology*, **30**, 227–230.

Ando, A., Kaiho, K., Kawahata, H. & Kakegawa, T. 2008. Timing and magnitude of early Aptian extreme warming: unraveling primary $\delta^{18}O$ variation in indurated pelagic carbonates at Deep Sea Drilling Project site 463, central Pacific Ocean. *Palaeogeography, Palaeoclimatology, Palaeoecology*, **260**, 463–476.

Bralower, T. J., CoBabe, E., Clement, B., Sliter, W. V., Osburn, C. L. & Longoria, J. 1999. The record of global change in mid-Cretaceous (Barremian-Albian) sections from the Sierra Madre, Northeastern Mexico. *Journal of Foraminiferal Research*, **29**, 418–437.

Chen, J. & Yang, H. 1996. Geological development of the northwest China basins during the Mesozoic and Cenezoic. *In*: Zhiyi, Z. & Dean, W. T. (eds) *Phanerozoic Geology of Northwest China*. Science Press, Beijing, 39–62.

Erba, E., Channell, J. E. T. *et al.* 1999. Integrated stratigraph of the Cismon APTICORE (Southern Alps, Italy): a reference section for the Barremian–Aptian interval at low latitudes. *Journal of Foraminiferal Research*, **29**, 371–391.

Frost, G. M., Coe, R. S. *et al.* 1995. Preliminary Early Cretaceous paleomagnetic results from Gansu Corridor, China. *Earth and Planetary Science Letters*, **129**, 217–232.

Gradstein, F. M., Ogg, J. G. & Smith, A. G. 2004. *A Geologic Time Scale*. Cambridge University Press, New York.

Grocke, D. R., Hesselbo, S. P. & Jenkyns, H. C. 1999. Carbon-isotope composition of Lower Cretaceous fossil wood: ocean–atmosphere chemistry and relation to sea-level change. *Geology*, **27**, 155–158.

He, H. Y., Wang, X. L., Zhou, Z. H., Wang, F., Boven, A., Shi, G. H. & Zhu, R. X . 2004. Timing of the Jiufotang Formation (Jehol Group) in Liaoning, northeastern China, and its implication. *Geophysical Research Letters*, **31**, L12605.

Heimhofer, U., Hochuli, P. A., Burla, S., Andersen, N. & Weissert, H. 2003. Terrestrial carbon-isotope records from coastal deposits (Algarve, Portugal): a tool for chemostratigraphic correlation on an intrabasinal and global scale. *Terra Nova*, **15**, 8–13.

Hollander, D. J. & McKenzie, J. A. 1991. CO_2 control on carbon-isotope fractionation during aqueous photosynthesis: a paleo-pCO_2 barometer. *Geology*, **19**, 929–932.

Jahren, A. H., Arens, N. C., Sarmiento, G., Guerrero, J. & Amundson, R. 2001. Terrestrial record of methane hydrated dissociation in the Early Cretaceous. *Geology*, **29**, 159–162.

Jenkyns, H. C. 2003. Evidence for rapid climate change in the Mesozoic–Paleogene greenhouse world. *Philosophical Transactions of the Royal Society A*, **361**, 1885–1916.

Ji, S.-A., Atterholt, J. *et al.* 2011. A new, three-dimensionally preserved enantiornithine bird (Aves: Ornithothoraces) from Gansu Province. *Zoological Journal of the Linnean Society*, **162**, 201–219.

Körner, C., Farquhar, G. D. & Roksandic, Z. 1988. A global survey of carbon isotope discrimination in plants from high altitude. *Oecologia*, **74**, 623–632.

Leng, M. J., Lamb, A. L. *et al.* 2006. Isotopes in lake sediments. *In*: Leng, M. J. (ed.) *Isotopes in Palaeoenvironmental Research. Developments in Palaeoenvironmental Research*. Springer, Dordrecht, 147–184.

Li, H. & Yang, J. 2004. Evidence for Cretaceous uplift of the northern Qinghai-Tibetan Plateau. *Earth Science Frontiers*, **11**, 345–359.

Ludvigson, G. A., Gonzalez, L. A., Kirkland, J. I., You, H.-L., Ufnar, D. F., Carpenter, S. J. & Davis, J. 2005. Stable isotope palaeorecords, Early Cretaceous Yixian Fm. (Barremian), Liaoning Province, P.R. China: paleohydrologic and paleoenvironmental interpretations. *Geological Society of America Abstracts with Programs*, **37**, 458.

Ludvigson, G. A., Joekel, R. M. *et al.* 2010. Correlation of Aptian–Albian carbon isotope excursions in continental strata of the Cretaceous foreland basin, Eastern Utah, U.S.A. *Journal of Sedimentary Research*, **80**, 955–974.

Menegatti, A. P., Weissert, H., Brown, R. S., Tyson, R. V., Farrimond, P., Stasser, S. & Caron, M. 1998. High-resolution $\delta^{13}C$ stratigraphy through early Aptian 'Livello Selli'. *Paleoceanography*, **13**, 530–545.

Ogg, J. G., Ogg, G. & Gradstein, F. M. 2008. *The Concise Geologic Time Scale*. Cambridge University Press, Cambridge.

Price, G. D. 2003. New constraints upon isotope variation during the early Cretaceous (Barremian–Cenomanian) from the Pacific Ocean. *Geology Magazine*, **140**, 513–522.

Robinson, S. A. & Hesselbo, S. P. 2004. Fossil-wood carbon-isotope stratigraphy of the non-marine Wealden Group (Lower Cretaceous, southern England). *Journal of the Geological Society, London*, **161**, 133–145.

Strohmenger, C. J., Steuber, T., Ghani, A., Barwick, D. G., Al-Mazrooei, S. H. A. & Al-Zaabi, N. O. 2010. Sedimentology and chemostratigraphy of the Hawar and Shu'aiba depositional sequences Abu Dhabi, United Arab Emirates. *GeoArabia Special Publication*, **4**, 341–365.

Talbot, M. R. 1990. A review of the paleohydrological interpretation of carbon and oxygen isotope rations in primary lacustrine carbonate. *Chemical Geology*, **80**, 261–280.

Talbot, M. R. & Kelts, M. 1986. Primary and diagenetic carbonates in the anoxic sediments of Lake Bosumtwi, Ghana. *Geology*, **14**, 912–916.

Tang, F., Luo, Z.-X., Zhou, Z.-H., You, H.-L., Georgi, A., Tang, Z.-L. & Wang, X.-Z . 2001. Biostratigraphy and palaeoenvironment of the dinosaur-bearing sediments in Lower Cretaceous of Mazongshan area, Gansu Province, China. *Cretaceous Research*, **22**, 115–129.

TSCreator 2011. Time Scale Creator visualization of enhanced Geologic Time Scale 2004 database (Version 4.2.5; 2011). James Ogg (database coordinator) and Adam Lugowski (software developer). World Wide Web Address: http://www.tscreator.org

van Breugel, Y., Schouten, S., Tsikos, H., Erba, E., Price, G. D. & Sinninghe Damste, J. S. 2007. Synchronous negative carbon isotope shifts in marine and terrestrial biomarkers at the onset of the early Aptian ocean anoxic event 1a: evidence for the release of 13-C depleted carbon into the atmosphere. *Paleoceanography*, **22**, PA 1210.

Van de Water, P. K., Leavitt, S. W. & Betancourt, J. L. 1994. Trends in stomatal density and $^{13}C/^{12}C$ ratios of Pinus flexilis needles during Last Glacial–Interglacial cycle. *Science*, **264**, 239–243.

Weissert, H. & Erba, E. 2004. Volcanism, CO_2 and paleoclimate: a Late Jurassic–Early Cretaceous carbon and oxygen isotope record. *Journal of the Geological Society, London*, **161**, 695–702.

You, H.-L., Atterholt, J., O'Connor, J. K., Harris, J. D., Lamanna, M. C. & Li, D.-Q. 2010. A second Cretaceous ornithuromorph bird from the Changma Basin, Gansu Province, northwestern China. *Acta Palaeontologica Polonica*, **55**, 617–625.

You, H.-L, Lamana, M. C. *et al.* 2006. A nearly modern amphibious bird from the early Cretaceous of northwest China. *Science*, **312**, 1640–1643.

You, H.-L., O'Conner, J., Chiappe, L. M. & Qiang, J. 2005. A new fossil bird from the early Cretaceous of Gansu Province, northwest China. *Historical Biology*, **17**, 7–14.

Zeng, L., Yang, J. & Li, H. 2006. Genesis of the Cretaceous HFSE-enriched Hongliuxia andesitic dike on the northern margin of the Qinghai-Tibet Plateau: anorthite fractional crystallization and enhanced dissolution of zircon. *Geology in China*, **33**, 326–331.

Zhao, X., Coe, R. S., Glider, S. A. & Frost, G. M. 1996. Palaeomagnetic constraints on the paleogeography of China: implications for Gondwanaland. *Australian Journal of Earth Sciences*, **43**, 643–672.